The radio properties of the cD galaxy of Abell 2390

Pedro Augusto,[1,2][*] Alastair C. Edge[3] and Claire J. Chandler[4]

[1]*Centro de Astrofísica da Universidade do Porto, Rua do Campo Alegre, 823, 4150 Porto, Portugal*

[2]*Universidade da Madeira, Centro de Ciências Matemáticas, Caminho da Penteada, 9050 Funchal, Portugal*

[3]*University of Durham, Department of Physics, South Road, Durham DH1 3LE*

[4]*National Radio Astronomy Observatory, PO Box O, Socorro, NM 87801,USA*

ABSTRACT

We present multifrequency, multi-epoch radio imaging of the complex radio source B2151+174 in the core of the cluster, Abell 2390 ($z \simeq 0.23$). From new and literature data, we conclude that the Faranoff–Riley type II (FRII)-powerful radio source is the combination of a compact, core-dominated 'medium-sized symmetric object' (MSO) with a more extended, steeper spectrum mini-halo. B2151+174 is unusual in a number of important aspects. (i) It is one of the most compact and flat spectrum sources in a cluster core known; (ii) it shows a complex, compact twin-jet structure in a north–south orientation; (iii) the orientation of the jets is 45° misaligned with apparent structure (ionization cones and dust disc) of the host galaxy on larger scales. Since the twin-jet of the MSO has its northern half with an apparent 'twist', it might be that precession of the central supermassive black hole explains this misalignment. B2151+174 may be an example of the early stage (10^3–10^4 yr duration) of a 'bubble' being blown into the intracluster medium where the plasma has yet to expand.

Key words: galaxies: active – galaxies: clusters: individual: Abell 2390 – galaxies: elliptical and lenticular, cD.

1 INTRODUCTION

The cores of clusters of galaxies host many of the most luminous radio sources in the local Universe (e.g. Cygnus-A, Hercules-A, Hydra-A). The influence of such powerful sources of radiation and mechanical energy on the surrounding intracluster medium (ICM) is clear in the core of the Perseus cluster (Böhringer et al. 1993; Fabian et al. 2003) and may be a significant energy source regulating cooling flows (Soker et al. 2001; Brüggen & Kaiser 2002; Fabian et al. 2002; Ruszkowski & Begelman 2002). The majority of this energy is believed to be injected into the ICM through mechanical work done by radio jets but relatively few cooling flows have luminous, lobed radio emission, and most are relatively compact and have low luminosity. This is as would be expected if these radio sources have a duty cycle of the order of 10^8 yr (Dalla Vecchia et al. 2004) but in a large sample of clusters a few luminous, compact sources should be found that are in the process of launching jets. With a view to investigating the influence of more compact radio sources on the ICM, we have undertaken an extensive, high-resolution radio imaging campaign of the radio source B2151+174 (Browne et al. 1998) that lies in the central galaxy of the rich cluster, Abell 2390. This cluster has a high X-ray luminosity ($L = 2.125 \times 10^{45}$ erg s^{-1}, 0.1–2.4 keV – Ebeling et al. 1996) and is known

to contain a cooling flow [$\lesssim$300 M$_\odot$ yr^{-1} (Allen, Ettori & Fabian 2001) from recent *Chandra* observations]. The central host galaxy of B2151+174 has extended optical emission lines (Le Borgne et al. 1991), extended Lyman α (Hutchings & Balogh 2000), strong dust absorption in the optical and submillimetre (sub-mm) dust continuum emission (Edge et al. 1999). B2151+174 is one of the most luminous radio sources in brightest cluster galaxies (BCG) (FRII 1.4-GHz power of $10^{25.1}$ W Hz^{-1}) in the combined brightest cluster sample (BCS)/extended brightest cluster sample (eBCS) X-ray flux-limited sample of 300 clusters (Ebeling et al. 1998, 2000) and samples of radio sources in cluster cores (Ball, Burns & Loken 1993) but the radio properties of B2151+174 differentiate it from most canonical central cluster radio sources. It has an apparently self-absorbed radio spectrum (Edge et al. 1999) implying that the majority of the radio emission is from a very compact region.

The kpc-scale radio structure of B2151+174 was unveiled for the first time by Augusto, Wilkinson & Browne (1998) from Very Long Baseline Array (VLBA) and Multi-Element Radio-Linked Interferometer Network (MERLIN) 5-GHz maps, who studied it as a candidate compact-symmetric object (CSO). In fact, in this paper, we revise the classification and find the source to be larger than 1 kpc, making it a medium-sized symmetric object (MSO). CSOs (sizes on 1–1000 pc) are radio sources with lobes on either side of a compact core which dominates at high frequencies (e.g. Wilkinson et al. 1994). MSOs are similar but larger (1–15 kpc). CSOs, short and 'twin-sided', are likely young sources (10^3–10^4 yr); the ages

[*]E-mail: augusto@uma.pt

Table 1. The radio observations of B2151+174, Right ascension (RA) (2000) = $21^h53^m36\overset{s}{.}8267$, declination (Dec.) (2000) = $+17°41'43\overset{''}{.}726$, ordered chronologically. All are continuum observations; for the VLA we indicate the configuration used. The observing time is given 'on-source' since for phase-referenced observations the actual total run was longer. The resolutions presented here are just approximate. When others used the same data, we give the relevant reference.

Telescope	Observing date	Integration time (on-source)	Phase-referenced observations?	Frequency (GHz)	Resolution (arcsec)	Reference
VLA-A	1992 October 18	2 min	Yes	8.4	0.2	Browne et al. (1998)
VLA-D	1993 September 7	10 s	Yes	1.4	45	Condon et al. (1998)
MERLIN	1995 June 4	80 min	Yes	5.0	0.05	Augusto et al. (1998)
MERLIN	1996 May 15	4 h	'Yes' (failed)	23	0.015	
VLBA+Y	1996 July 25	1 h	No	5.0	0.003	Augusto et al. (1998)
MERLIN plus EVN[a]	1997 May 30	1.5 h	yes	1.7	0.02	
VLA-DnC	1997 October 22	16 min	Yes	1.4	226.0	Edge et al. (1999)
VLA-DnC	1997 October 22	16 min	Yes	4.85	210.8	Edge et al. (1999)
VLA-DnC	1997 October 22	6 min	Yes	8.4	139.4	Edge et al. (1999)
VLA-DnC	1997 October 22	19 min	Yes	15	101.1	Edge et al. (1999)
VLA-DnC	1997 October 22	26 min	Yes	22	73.2	Edge et al. (1999)
VLA-DnC	1997 October 22	37 min	Yes	43	41.7	Edge et al. (1999)
VLA-A	2002 February 12	2 min	No	43	0.06	
VLA-B	2004 May 9	≈1 h	Yes	0.074	80	lwa.nrl.navy.mil/VLSS

[a]The MERLIN plus EVN used the following telescopes: LoDeCbKnDaMkTa plus EfJbCbMcNtOnWbTr.

of some have been determined by either kinematical studies (e.g. Owsianik, Conway & Polatidis 1998) or synchrotron emission ageing (Readhead et al. 1996).

In Section 2, we present the process of data collection and describe its processing, including the problems found. In Section 3, we use all the data to make an extensive study of the radio properties of B2151+174, from maps, spectra (total and main components), variability (or lack of it), jets orientation, size, mini-halo evidence, etc. Finally, in Section 4, we conclude this paper with an overall discussion. Throughout this paper, we assume $H_0 = 75$ km s^{-1} Mpc^{-1}, $q_0 = 0.5$ and $\Lambda = 0$.

2 OBSERVATIONS AND DATA REDUCTION

B2151+174 was observed by us with several radio interferometer arrays as detailed in Table 1. All radio data were processed using AIPS (National Radio Astronomy Observatory) and DIFMAP (CalTech package) through the standard routines. During the observations, we used the standard point source and flux calibrators (except for MERLIN 23 GHz as noted below) as well as fringe finders for the very long baseline interferometry (VLBI) (VLBA and European VLBI Network – EVN) observations and a nearby phase-referencing calibrator for some of the observations (see Table 1).

Although we had same epoch MERLIN plus EVN 18-cm observations (Table 1), we have preferred to keep them separate (MERLIN and EVN) on the context of the detailed analysis done in Section 3.

Augusto et al. (1998) have studied B2151+174 as part of a radio search for gravitational lenses. They presented two C-band (5-GHz) maps: one with MERLIN 5 GHz and the other with VLBA 5 GHz. We have re-reduced the Augusto et al. 5-GHz data and obtained consistent results. We have also re-reduced the Very Large array (VLA)-A 8.4-GHz data from the Jodrell–VLA Astrometric Survey (JVAS; Browne et al. 1998).

We have produced new MERLIN 23-GHz self-calibrated maps from data mentioned by Augusto et al. (1998) which had poor phase reference, and self-calibration was not attempted given that the aim of that paper was a lens search. We believe the phase referencing was unsuccessful because the map position is actually about 120 mas off the known ~mas-precision position that we use throughout

this paper (from VLA-A 8.4-GHz data – Browne et al. 1998). As regards the flux density calibration, unfortunately, the standard 3C 286 flux calibrator was not observed. Instead, the highly variable point-source calibrator 3C 273 was used. Flux monitoring of this source made with MERLIN at the time, give or take a few days, gave too high a flux density value for B2151+174 when compared with other K-band data that we have also collected (see below). This calibration problem affects all Augusto et al. MERLIN 23-GHz observations, although we are confident that they have presented trustworthy maps of the five other sources. Judging from their overall spectra alone, however, of the five sources in Augusto et al. (1998), two seem to have a too high flux density point from MERLIN 23 GHz in the rough proportion that our B2151+174 value is high. For the quantitative results of Section 3, we recalibrated these MERLIN 23-GHz data using our VLA-DnC 22-GHz measurements (Table 1) by dividing the initial flux densities by 3.05.

We have decided to either use maximum resolution (uniform weighting of baselines) or use maximum sensitivity (natural weighting), depending on the best option for the detailed component analysis that followed. These were as follows. (i) Uniform weighting – MERLIN 1.7 GHz, VLA-A 8.4 and 43 GHz; (ii) natural weighting – EVN 1.7 GHz, MERLIN 5 and 23 GHz, and VLBA 5 GHz. In all maps produced, we have used the 3σ level for the lowest contour (where σ is the rms on the map shown, in each case, at the relevant caption). See Table 2, which contains all map details.

3 RADIO PROPERTIES OF THE cD GALAXY

We have model fitted all maps in DIFMAP and present the resulting models in Table 3. With the objective of a confident description of the structure and spectra of the B2151+174 components, we were careful to use several ways of checking that the models were sensible: (i) using DIFMAP to inspect how well the model was fitting the data both in visibility and in residuals; (ii) plotting the corresponding maps and comparing them with the ones obtained by the CLEANing process in DIFMAP (Figs 1 and 2); (iii) comparing the rms of the CLEANed maps with the rms of the maps obtained with the corresponding models: the models all have an rms which is within 50 per cent of the one of the CLEANed maps. For models with

Table 2. The details for each of the maps of B2151+174 in Figs 1 and 2. The contours are drawn in powers of two from the first one. Note that the peak flux density always decreases with smaller beam size.

Instrument	Frequency (GHz)	Figure	Beam (×0.001 arcsec)	Peak (mJy beam^{-1})	First contour (3σ) (per cent)	Total flux density (mJy)
MERLIN	1.7	1(c)	90 × 90	141	0.7	219 ± 20
EVN	1.7	2(c)	20 × 20	62	2	171 ± 26
MERLIN	5.0	1(a)	70 × 70	168	0.33	199 ± 20
VLBA	5.0	2(a)	2.5 × 2.5	115	0.5	157 ± 14
VLBA	5.0	2(b)	10 × 10	128	0.5	157 ± 14
VLA-A	8.4	1(d)	90 × 90	116	0.7	134 ± 23
MERLIN	23	2(d)	15 × 15	45^a	2.5	73^a ± 24
VLA-A	43	1(b)	40 × 40	45	8.5	61 ± 15

^{a}Recalibrated flux density values (see Section 2).

Table 3. The models fitted to all radio data with maps in Figs 1 and 2. For each gaussian component, S is the flux density, r and θ describe the separation vector from the origin, a is the major axis, b/a is the axial ratio and Φ is the PA of elongation. Finally, χ^2 is the error in the fitting, well described in Polatidis et al. (1995): if less than one the model is fine. The components on which we are most confident for spectra and morphology analysis are labelled with the corresponding letter (in the final column) as in the maps.

S (mJy)	r (mas)	θ (°)	a (mas)	b/a	Φ (°)	χ^2 component
		MERLIN	1.7 GHz			0.73
138	0.0	0.0	65.1	0.00	16.6	N-large
35	140.9	174.3	116.7	0.64	−5.5	C
23	155.2	5.8	127.3	0.82	−44.0	B
15	187.2	−152.2	298.8	0.67	70.9	
7	285.1	176.4	310.6	0.00	−22.7	
		EVN	1.7 GHz			2.26
63	0.0	0.0	7.3	0.13	56.2	N-small
40	44.8	6.4	60.2	0.25	17.3	
20	73.2	160.3	78.7	0.10	20.0	
18	171.3	−0.6	26.7	0.67	7.3	
12	196.8	165.2	116.3	0.00	−27.6	
10	237.9	−5.8	114.6	0.00	−22.7	
		MERLIN	5.0 GHz			0.72
164	0.0	0.0	16.3	0.00	0.4	N-large
25	64.2	1.1	52.7	0.00	0.33	A
7	141.2	176.6	60.7	0.17	−21.0	C
4	269.7	−0.4	192.9	0.00	−6.3	
		VLBA	5.0 GHz			2.33
121	0.0	0.0	0.8	0.32	−3.9	N-small
30	80.0	1.4	50.0	0.1	−26.0	
8	4.7	179.0	2.2	0.38	−10.6	
		VLA-A	8.4 GHz			0.00058
115	0.0	0.0	49.6	0.00	−9.2	N-large
9	78.3	42.5	182.0	0.00	11.5	
8	153.0	167.5	200.9	0.32	10.1	C
5	160.2	3.6	251.1	0.00	−8.4	
		MERLIN	23 GHz			0.33
48^a	0.0	0.0	8.0	0.57	16.3	N-small
15^a	104.8	22.9	11.5	0.66	−25.8	
8^a	9.7	−32.4	11.9	0.00	−12.0	
		VLA-A	43 GHz			0.36
42	0.0	0.0	15.3	0.15	11.2	N-small
6	64.7	−21.8	83.8	0.00	−77.9	A

^{a}Recalibrated flux density values (see Section 2).

$\chi^2 > 1$ (VLBA 5 GHz and EVN 1.7 GHz), only the strongest (nuclear) component was used in this section. Furthermore, in the following subsections we have not considered the components that had: (i) a surface brightness less than 20 times the rms surface brightness (for which we used the beam sizes); (ii) a fitted axial ratio of zero, *unless* they were a nuclear component or the semimajor axis of the component was smaller than the semimajor axis of the respective beam. Apart from the nucleus (clearly identified in *all* data sets), we only used three components (labelled A, B and C; see Table 3). When the fitted ellipses intersected, we cross-identified the same component in different data sets (see Fig. 1).

3.1 Morphology

The closest component to the nucleus is A, seen in both MERLIN 5-GHz and VLA-A 43-GHz data [see Figs 1(a) and (b); Table 3]. Making the average between both models, this component is ~64 mas (~0.20 kpc) from the nucleus[1] at position angle (PA) $\simeq −11°$ and compact (smaller than the formal resolution of both data sets and with 0.00 fitted axial ratios). Further away and on the east side of north resides component B, only identified with MERLIN 1.7 GHz [Fig. 1(c); see also Table 3]. This one is ~155 mas (~0.48 kpc) from the nucleus at PA $\simeq +6°$ and is clearly resolved [an almost circular 'blob' ~127 mas (~0.40 kpc) in diameter]. Finally, on the other side of the nucleus and at a similar distance (but not quite opposed) lies component C, seen with MERLIN 1.7 and 5 GHz and VLA-A 8.4 GHz [Figs 1(a), (c) and (d)] ~145 mas (~0.45 kpc) away from the nucleus at PA $\simeq +173°$ (again taking the average values). This is also a resolved 'blob', although the different resolutions cannot clearly reveal its size; it is elliptical in shape [somewhere on ~60–200 mas (~0.2–0.6 kpc) with a 0.2–0.6 axial ratio].

As regards the three highest resolution maps (EVN 1.7 GHz, VLBA 5.0 GHz and MERLIN 23 GHz – Fig. 2), the structures seen support the overall double-and-opposite-jet structure seen with the labelled components: the MERLIN 23-GHz map hints at a bending jet, starting off at the NW and bending afterwards to NE; the EVN 1.7-GHz map is consistent with this, but only shows larger scale structure on both sides of the nucleus: towards SE and towards NE – most components are too resolved; the VLBA 5.0-GHz map, with a finer resolution than any of the previous ones, similarly to the EVN data hints at a bending northern jet, starting off at the NW

---

[1] In all that follows we assume the radio structure to be perpendicular to our line of sight, that is, parallel to the plane of the sky, so all quoted distances are linear *projected* distances.
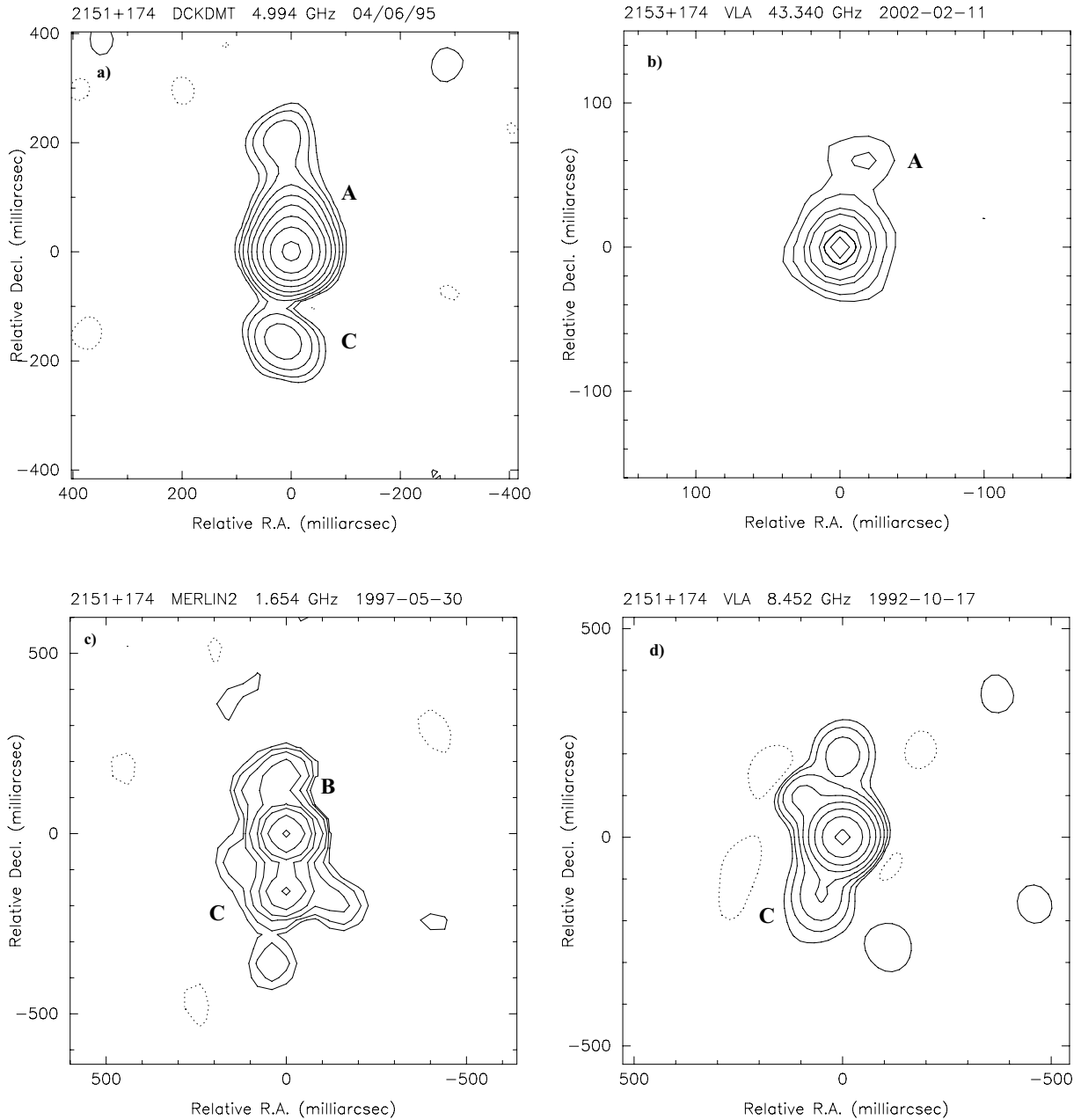
Figure 1. The maps produced with all B2151+174 data containing labelled non-nuclear components as in Table 3: (a) MERLIN 5-GHz map, as in Augusto et al. (1998) but convolved with a 70-mas circular beam; (b) VLA-A 43-GHz map where the data were convolved with a 40-mas circular beam; (c) MERLIN 1.7-GHz map; the data were convolved with a 90-mas circular beam (super-resolved by a factor of 1.3–2, depending on direction); (d) VLA-A 8.4-GHz map with the data convolved with a 90-mas circular beam (super-resolved by a factor of 1.9–2.3, depending on direction). See Table 2 for the details of each map.

and bending through north: from the (smaller) distances of the components seen, the whole picture is consistent with both the MERLIN 23-GHz and EVN 1.7-GHz maps. Finally, the VLBA 5.0-GHz map also shows, very close to the nucleus, a SE pointing jet.

B2151+174 can be classified as a small bright core MSO, given its triple-component structure which is dominated by a bright core (e.g. Augusto et al. 1998, 1999). Using the same '5-GHz 6σ' size definition for CSO/MSOs of Augusto et al. (2006), the MERLIN 5.0-GHz map implies an angular size of 0.49 arcsec for B2151+174 or 1.5 kpc at its $z = 0.2302$ (Le Borgne et al. 1991; Yee et al. 1996). In fact, at 1.7 GHz with MERLIN the size is almost twice, using the same convention (2.7 kpc).

3.2 The spectra of B2151+174 and its main components

We have measured the total flux density of B2151+174 for all continuum data presented in Table 1 and show the thus compiled spectra in Fig. 3. In this same figure, we also include, from the literature, the following points (in order of frequency): 74 MHz [VLA Low-frequency Sky Survey (VLSS)], 365 MHz (Douglas et al. 1996), 408 MHz (Dixon 1970), 1400 MHz (White & Becker 1992; Condon et al. 1998) and 4850 MHz (Gregory & Condon 1991).

The overall shape of the spectrum is typical of a two-component source, containing a compact portion (dominant at high frequencies and responsible for the flat $\alpha_{0.365}^{43} \simeq 0.47$) and a very extended one
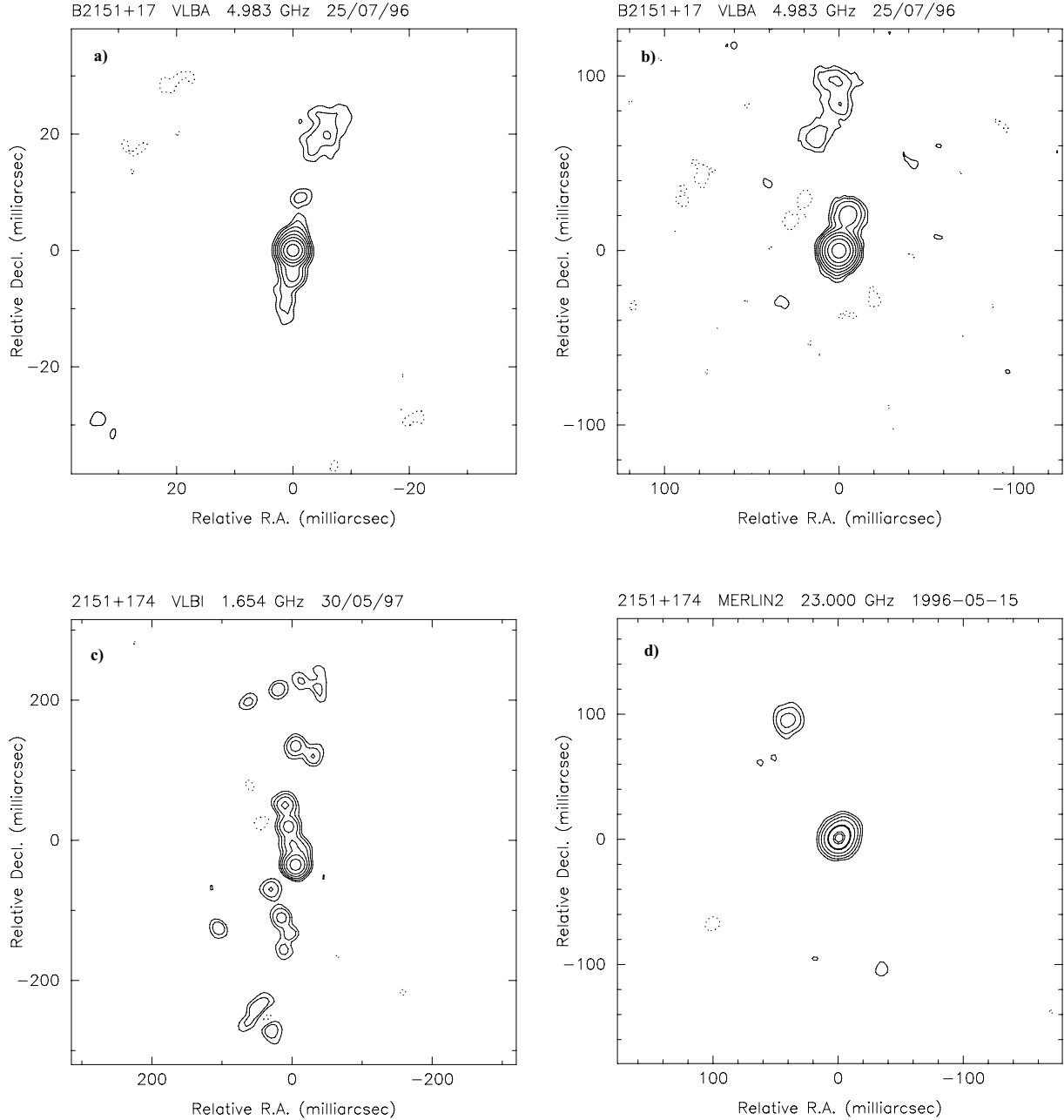
Figure 2. The maps produced with all B2151+174 data with only nuclear components labelled in Table 3: (a) VLBA 5-GHz map, with the data convolved with a 2.5-mas circular beam – only the central nuclear region is shown; (b) VLBA 5-GHz map produced by convolving the data with a 10-mas circular beam; the central region (shown in panel a) is at the centre; (c) EVN 1.7-GHz map with a 20-mas circular beam; (d) MERLIN 23-GHz map with a 15-mas circular beam. See Table 2 for the details of each map.

(dominant at low frequencies and responsible for the steep $\alpha_{74}^{365} \simeq 1.10$). The first is the MSO part, described in detail in the previous section, while the latter is the mini-halo, described in Section 3.6. The spectra, again, become steeper on the way to high-ν radio and sub-mm wavelengths where $\alpha \sim 0.7$–0.9 (Edge et al. 1999).

To get spectral information on the several components of B2151+174, we must decide first on how to superpose the different frequency maps. In an ideal situation, one would like to have all maps properly phase-referenced and also same epoch. This is not the case, since the data are both sparse in epochs (a rough 10-yr span from the earliest through the latest data) and also not all were phase-referenced to a calibrator (Table 1), and for some of the ones

which were it is not clear that this has worked properly. Hence, since this is a source that is core-dominated at all frequencies observed (except the lowest – 74 MHz), we assume that it is safe to take the brightest component on all maps as the central nucleus.

Proceeding from this assumption, we can now 'superpose' all maps (in fact, the component positions of Table 3) to get spectral information for three components: nucleus (N), A and C. We have preferred not to do this in the standard way of producing spectral index maps for two reasons. First, we have too many frequencies to play with, and spectral index maps are (usually) made only between two frequencies. This would imply too many spectral index maps to interpret for such a relatively simple (and weak) radio source.
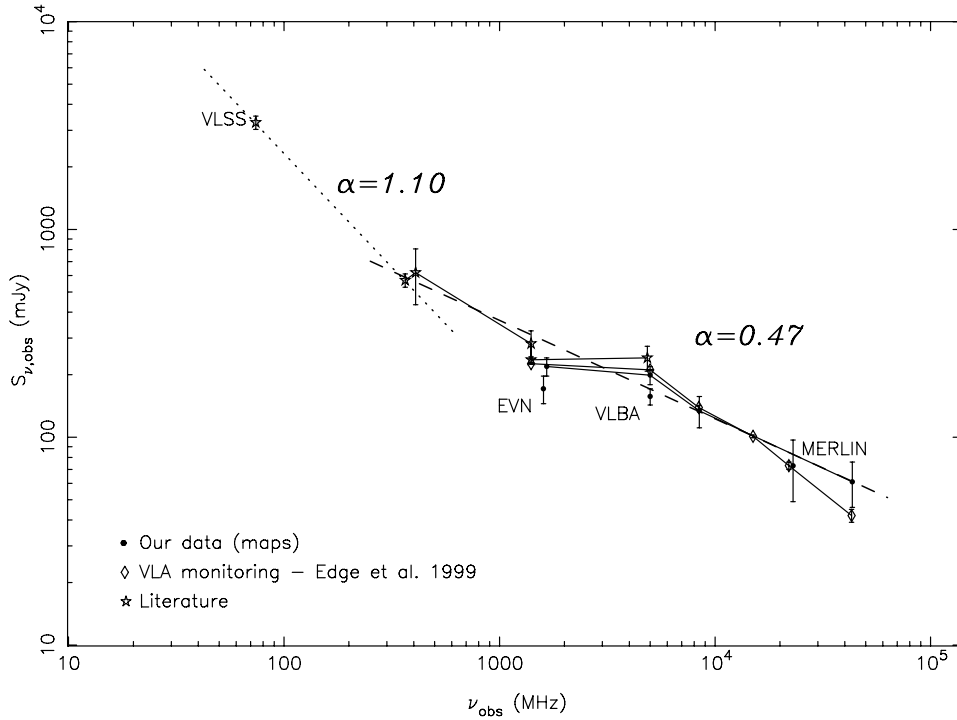
Figure 3. The total spectra of B2151+174. In this plot, we show all available data points from three different sources: first, from our data (Table 1 and Section 3.1); secondly, from the VLA monitoring, we conducted with results published in Edge et al. (1999); finally, from the literature, whose different references are given in the text. There are some other notes worthy of mention. First, note the three points that are not connected with lines and correspond to high-resolution observations (EVN, VLBA and MERLIN 23 GHz) which missed extended structure seen with MERLIN at 1.7 and 5 GHz (black circles with lines connected). Our VLA-A 8.4-GHz measurement (134 ± 23 mJy) is entirely consistent with the one of Browne et al. (1998), 129 mJy and with Edge et al. (1999) VLA-DnC monitoring. Except for the three noted high-resolution points and the VLSS one, we have used all the remaining to fit the dashed line shown, getting $\alpha \simeq 0.47$ ($r^2 = 0.838$), $S_\nu \propto \nu^{-\alpha}$. Finally, in a dotted line, we also present the two-point $\alpha_{74}^{365} \simeq 1.10$, which is consistent with a mini-halo in Abell 2390 (see Section 3.6).

Secondly, related to this weakness of the structure, none of our data sets was actually a full run of observations. Most were short shapshots with poor $u-v$ coverage (the poor quality of the data is reflected in the ~40 per cent of the components in Table 3 which are not labelled).

Since the nuclear component in model fitting had its flux density measured by seven instruments with a range of resolution spanning nearly two orders of magnitude (translating into the very different physical sizes), we found it better to split it into the 'compact nucleus' (N-small), using EVN, VLBA, MERLIN 23-GHz (recali-

brated – see Section 2) and VLA-A 43-GHz data and the 'extended nucleus' (N-large), using the remaining data. In Fig. 4, we present the spectra of both approaches. The characteristic GHz-peaked spectrum for N-small leaves no room for doubt that this is a typical active galactic nucleus (AGN).

For component A, we actually have two data points (MERLIN 5 GHz and VLA-A 43 GHz) which give ($S_\nu \propto \nu^{-\alpha}$): $\alpha_{5.0}^{43}$ (A) = 0.66 ± 0.2 [cf. $\alpha_{5.0}^{43}$ (N) = 0.63 ± 0.2]. Finally, component C has three-frequency data points (MERLIN 1.7 and 5.0 GHz and VLA-A 8.4 GHz), but the highest frequency points are both weak (<10 mJy)
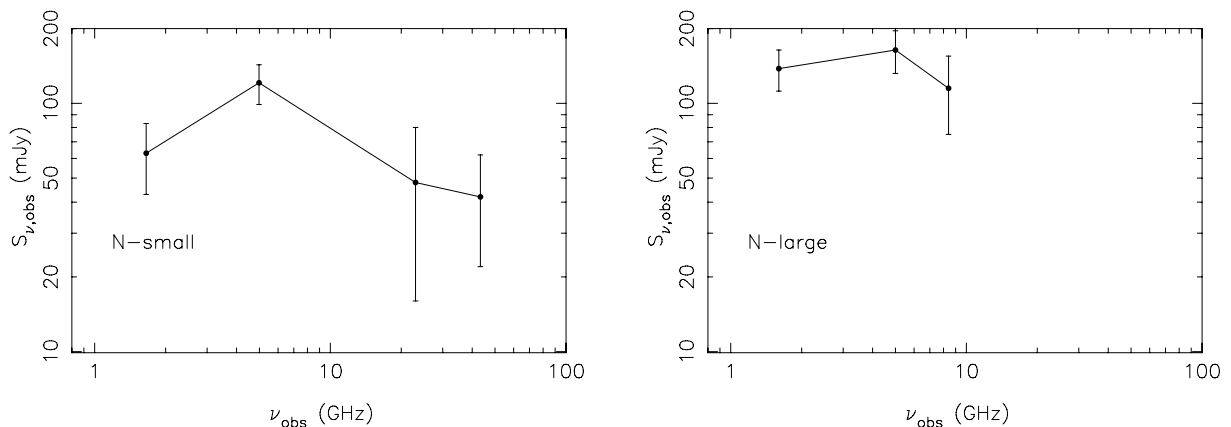

Figure 4. The spectrum of the nucleus of B2151+174 as model fitted using EVN 1.7-GHz, VLBA 5-GHz, MERLIN 23-GHz (recalibrated – see Section 2) and VLA-A 43-GHz data (N-small) or using MERLIN 1.7-GHz, MERLIN 5-GHz and VLA-A 8.4-GHz data (N-large).

Table 4. The physical parameters of the four labelled components (column 1) of Table 3 with spectral information in Section 3.2, including the nuclear component N split into two. We have used the most appropriate data sets (column 2), given the flux density/frequency data points (columns 9–10) available for each component spectra: the spectral indices (column 8) were calculated between the shown frequencies, the best approximation possible for the formal calculation between ν_{hi} and ν_{lo} (columns 6–7) . These are, respectively, the two cut-off frequencies (which eventually might be) seen in the spectra of each component, the former one most crucial, indicative of spectral ageing and giving a more accurate calculation of the sychrotron age of the emitting electrons (column 13). For the calculation of this t_{sync} we have guessed $\nu_{hi} = 100$ GHz for all components. We had to do the same for the calculation of the minimum energy magnetic field (column 11) and also further assume a ν_{lo} for the non-nuclear components. This calculation also required, apart from the assumptions in the text, the major (θ_x; column 3) and minor (θ_y; column 4) axis of each component as well as the guessed physical linear depth $s = \theta_y$ (column 5). Finally, in column 12, we also present the minimum energy density.

(1)	(2)	(3)	(4)	(5)	(6)	(7)	(8)	(9)	(10)	(11)	(12)	(13)
Component	Data	θ_x (arcsec)	θ_y (arcsec)	s (kpc)	ν_{hi} (GHz)	ν_{lo} (GHz)	$\alpha_{\nu_{lo}}^{\nu_{hi}**}$	ν_0 (GHz)	S_{ν_0} (Jy)	B_{me} (μG)	u_{me} (erg cm^{-3})	t_{sync} (yr)
N-small	VLBA 5 GHz	0.0008	0.00026	0.00081	100	5	0.52_5^{43}	4.983	0.121	5×10^2	2×10^{-8}	1×10^4
N-large	VLA-A 8.4 GHz	0.0496	0.000496	0.00154	100	5	$0.68_5^{8.4}$	8.452	0.115	1×10^2	1×10^{-9}	1×10^5
A	VLA-A 43 GHz	0.0838	0.000838	0.0026	100	0.1	0.66_5^{43}	43.34	0.006	6×10^1	3×10^{-10}	3×10^5
C	MERLIN 5 GHz	0.0607	0.0103	0.032	100	0.01	$1.46_{1.7}^5$	4.994	0.007	3×10^1	1×10^{-10}	7×10^5

and similar. Hence, we do not plot its spectra but rather get $\alpha_{1.7}^{5.0}$ (C) $= 1.46 \pm 0.2$. Thus, it seems that the south component is dominated by a lobe-like steep spectrum structure (C) while the north shows a compact 'knot' (A) on the way to another probable lobe-like structure (B) that we cannot confirm for the lack of data. All in all, it is very likely that the north jet of B2151+174 is slightly pointing towards us.

3.3 Variability

Our data support the conclusion of Edge et al. (1999) that there has been no significant variability in B2151+174 in the past 15 yr. Our highest resolution mapping also shows no significant displacement of the radio components in position (as would be expected for un-beamed jets viewed close to perpendicular to the line of sight). It is quite clear (Fig. 4) that 5 GHz is the ideal frequency to probe the compact nuclear component to test for variability in the future.

3.4 The age of the radio source and cooling flow timing

Assuming that the labelled component farthest from the nucleus is travelling at close to the speed of light (as would be expected from other powerful radio sources), then we can place a crude lower limit on the time-scale of the recent activity. Taking components B and C (both 0.15-arcsec or 0.45-kpc offset from the nucleus) as the most distant, then this limit is $\simeq 1.5 \times 10^3$ yr. If we take the estimated full size of B2151+174 (see end of Section 3.1) then this limit increases to $\simeq 4.5 \times 10^3$ yr.

To assess the validity of this limit, we need to determine the synchrotron radiation time-scale (t_{sync}). To do this, we must first get an estimate for the magnetic field/energy density (B_{me}/u_{me}) for each component assuming minimum energy (near equipartition of energy between relativistic particles and magnetic field), the same energy in heavy particles and electrons, a filling factor of *one* for the emitting electrons, cylindrical symmetry and an alignment of the magnetic field such that $\sin\phi = 1$ (Miley 1980), that is, the magnetic field is in the plane of the sky:

$$\begin{cases} B_{me} = 0.569 \left[2 \frac{(1+z)^{3+\alpha}}{\theta_x \theta_y s} \frac{S_{\nu_0}}{\nu_0^{-\alpha}} \frac{\nu_{hi}^{0.5-\alpha} - \nu_{lo}^{0.5-\alpha}}{0.5-\alpha} \right]^{2/7} \text{μG} \\ u_{me} = 9.28 \times 10^{-14} B_{me}^2 \text{ erg cm}^{-3} \quad (B_{me} \text{ in μG}), \end{cases}$$

with θ_x, θ_y the dimensions (in arcsec) of each component (model fitted – Table 3), $s = \min\{\theta_x, \theta_y\}$ (kpc) the path-length through the

source in the line of sight, z the redshift of the source (0.2302 in this case) and the remaining parameters refer to the spectra of the components, many of which had to be guessed; S_ν is in Jy and the ν is in GHz – more details are in the caption of Table 4 where we present the results. For the B_{me} calculation, components with fitted axial ratios (in the respective data set) of 0.00 had this changed to 0.01 (calculation of θ_y and s). The t_{sync} calculation was simplified from the formulae used (Murgia et al. 1999), ignoring expansion effects [B_{CMB} is the magnetic field equivalent to the cosmic microwave background (CMB) and equals $3.25(1 + z)^2$ in μG]:

$$t_{sync} = 1.610 \times 10^9 \frac{B_{me}^{0.5}}{B_{me}^2 + B_{CMB}^2} \frac{1}{\nu_{hi}^{0.5}(1 + z)^{0.5}} \text{ (yr)},$$

and we obtain, ignoring the CMB contribution and applying the redshift of B2151+174:

$$t_{sync} \simeq \frac{1.452 \times 10^9}{\nu_{hi}^{0.5} B_{me}^{1.5}} \text{ (yr) .}$$

This results in time-scales up to $\sim 7 \times 10^5$ yr, about two orders of magnitude higher than the crude expansion lower limit. This might be due to the presence of relevant expansion effects (e.g. Murgia et al. 1999).

The radio time-scales can also be estimated from the general properties of the larger cluster samples. Taking A2390 as a unique 'outbursting' source in the sample of Ball et al. (1993) then approximately 1 per cent of all cD galaxies are in this state at any one time. In the extreme limit of each system experiencing only one outburst in the look-back time range sampled (3×10^9 yr) then the average duration of these outbursts is $\sim 3 \times 10^7$ yr [comparable to the duration of injections assumed by Dalla Vecchia et al. (2004) of 10^7 yr]. If they happen more often, then this duration will be lower. Obtaining the statistics of a large and complete sample of central cluster radio sources with multifrequency radio mapping should allow much better limits on the time-scales of outbursts and their duty cycles.

3.5 The jet direction and galaxy structure

The orientation of the jet components close to north–south is in stark contrast to what is observed in *Hubble Space Telescope* (*HST*) images of the cD galaxy of Abell 2390 which show a biconical structure, strongly suggestive of nuclear ionization, oriented at PA $-45°$, the same orientation of a sharp linear dust lane that runs across
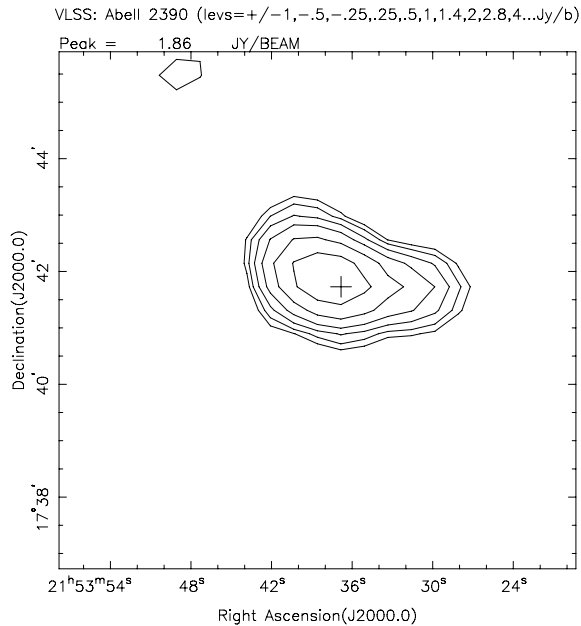
Figure 5. Abell 2390 as seen with the VLSS at 74 MHz (lwa.nrl.navy.mil/VLSS). The component is fitted with a ∼1.8-arcmin size in the east–west direction but has a still unknown size in the north–south direction (<0.7 arcmin).

the galaxy (Edge et al. 1999). One would expect the radio jet to lie in the same PA, between the projected limits of the ionization cone (e.g. Bremer, Fabian & Crawford 1997) but there is a 45° misalignment.

The most obvious explanation for this misalignment is that the structure seen in the *HST* imaging is related to a previous outburst when the jet was orientated differently. The precession of the supermassive black hole and associated accretion disc is possible. The displacement of component A from the near axisymmetry of the nucleus and components B and C (170° with respect to the nucleus) may be smaller scale evidence for such precession, as well as the twisting northern jet suggested by Figs 2(a)–(c), but the effects of beaming must be taken into account [e.g. from Fig. 1(a) and Table 2, $S_A/S_C \sim 4$].

3.6 The origin of steep spectrum emission

A recent VLSS 74-MHz map (Fig. 5) shows a significant, extended source [modelled as $\simeq 1.8 \times <0.7$ arcmin^2 in size; at the 0.228 redshift of Abell 2390 (Le Borgne et al. 1991; Yee et al. 1996) this translates into $\simeq 0.33 \times <0.12$ Mpc] with a flux density that lies well above the extrapolation of the spectral index of the components resolved at higher frequencies (Fig. 3). The extent to the west matches both the X-ray morphology, which shows an excess in this direction, and the lensing models, that show evidence for an additional mass component. This low-frequency emission is inconsistent with the low-frequency contribution from the 'N-large' components we resolve in this study (Fig. 4) but is consistent with the diffuse component found in the 1.4-GHz VLA map of Bacchi et al. (2003) that is too diffuse to be resolved in our observations. Assuming that the majority of the lowest frequency data arises from this diffuse component, then literature data give $\alpha_{74}^{365} \simeq 1.10$ (Fig. 3). This diffuse, steep spectrum component implies the presence of a mini-halo like the one observed in Perseus/3C84 (e.g. Pedlar et al. 1990; Silver, Taylor & Vermeulen 1998) and A2052/3C317 (Zhao et al. 1993;

Venturi, Dallacasa & Stefanachi 2004) and points to a history of activity in this system over a period much longer than the current event.

This result highlights the importance of low-frequency studies of cluster cores in addition to the more conventional higher frequency studies to gauge the power output and duty cycle of the radio sources that are purported to provide the energy required to reduce or balance cooling.

4 CONCLUSIONS

The radio source associated with the cD galaxy in the rich, X-ray luminous cluster A2390 (B2151+174) is unusual in a number of important aspects. First, it is one of the most compact and flat spectrum sources in a cluster core known. Secondly, it shows a complex, compact twin-jet structure. Thirdly, the orientation of the jets is not aligned with apparent structure of the host galaxy on larger scales.

These properties are intriguing given the recent realization that the influence of an AGN in the centre of a cluster could have a very significant impact on the ICM in the core and the suppression of cooling. B2151+174 may be an example of the early stage of a 'bubble' being blown into the ICM where the plasma is yet to expand. This initial phase will be relatively short (10^3–10^4 yr) compared to the later stages of the expansion (10^6–10^7 yr) so few 'young' sources can be expected in any selection of clusters.

It is important to note that the 1.4-GHz radio power of B2151+174 ($10^{25.1}$ W Hz^{-1}) is relatively small compared to the events that are thought to have an appreciable effect on the ICM in the core of a cluster (Dalla Vecchia et al. 2004) but the probability of observing the early stages of a sufficiently powerful event is small. In samples of clusters of galaxies at least 300 are needed before the meaningful statistics of these 'young' sources can be assessed as the 'outburst' period is a small fraction of the duration of each injection event. Alternatively, establishing what fraction of bright, compact GHz-peaked spectrum radio sources (the probable appearance of such sources) is in cluster cores would also provide important constraints on these issues.

Perhaps the most puzzling aspect of B2151+174 is the gross misalignment of the smallest scale radio jet with the larger scale 'ionization cones' and dust disc seen in *HST* imaging. This may simply result from precession of the central supermassive black hole between two distinct episodes of activity or indicate a complex change in the angular momentum of gas accreted in the inner part of the disc in this galaxy. High spatial resolution radio imaging of other systems in which a clear large-scale alignment is found will be important in addressing this issue.

operated as a National Facility by JBO, University of Manchester, on behalf of the UK Particle Physics & Astronomy Research Council.

REFERENCES

Allen S. W., Ettori S., Fabian A. C., 2001, MNRAS, 324, 877

Augusto P., Wilkinson P. N., Browne I. W. A., 1998, MNRAS, 299, 1159

Augusto P., Gonzalez-Serrano J. I., Edge A. C., Gizani N. A. B., Wilkinson P. N., Perez-Fournon I., 1999, New Astron. Rev., 43, 663

Augusto P., Gonzalez-Serrano J. I., Perez-Fournon I., Wilkinson P. N. 2006, MNRAS, submitted

Bacchi M., Feretti L., Giovannini G., Govoni F., 2003, A&A, 400, 465

Ball R., Burns J. O., Loken C., 1993, AJ, 105, 53

Böhringer H., Voges W., Fabian A. C., Edge A. C., Neumann D., 1993, MNRAS, 264, L25

Bremer M. N., Fabian A. C., Crawford C. S., 1997, MNRAS, 284, 213

Browne I. W. A., Patnaik A. R., Wilkinson P. N., Wrobel J. M., 1998, MNRAS, 293, 257

Brüggen M., Kaiser C. M., 2002, Nat, 418, 301

Condon J. J., Cotton W. D., Greisen E. W., Yin Q. F., Perley R. A., Taylor G. B., Broderick J. J., 1998, AJ, 115, 1693

Dalla Vecchia C., Bower R. G., Theuns T., Balogh M. L., Mazzotta P., Frenk C. S., 2004, MNRAS, 355, 995

Dixon R. S., 1970, ApJS, 20, 1

Douglas J. N., Bash F. N., Bozyan F. A., Torrence G. W., Wolfe C., 1996, AJ, 111, 1945

Ebeling H., Voges W., Böhringer H., Edge A. C., Huchra J. P., Briel U. G., 1996, MNRAS, 281, 799

Ebeling H., Edge A. C., Böhringer H., Allen S. W., Crawford C. S., Fabian A. C., Voges W., Huchra J. P., 1998, MNRAS, 301, 881

Ebeling H., Edge A. C., Allen S. W., Crawford C. S., Fabian A. C., Huchra J. P., 2000, MNRAS, 318, 333

Edge A. C., Ivison R. J., Smail I., Blain A. W., Kneib J.-P., 1999, MNRAS, 306, 599

Fabian A. C., Allen S. W., Crawford C. S., Johnstone R. M., Morris R. G., Sanders J. S., Schmidt R. W., 2002, MNRAS, 332, L50

Fabian A. C., Sanders J. S., Allen S. W., Crawford C. S., Iwasawa K., Johnstone R. M., Schmidt R. W., Taylor G. B., 2003, MNRAS, 344, L43

Gregory P. C., Condon J. J., 1991, ApJS, 75, 1011

Hutchings J. B., Balogh M. L., 2000, AJ, 119, 1123

Le Borgne J.-F., Mathez G., Mellier Y., Pelló R., Sanahuja B., Soucail G., 1991, A&AS, 88, 133

Miley G., 1980, ARA&A, 18, 165

Murgia M., Fanti C., Fanti R., Gregorini L., Klein U., Mack K.-H., Vigotti M., 1999, A&A, 345, 769

Owsianik I., Conway J. E., Polatidis A. G., 1998, A&A, 336, L37

Pedlar A., Ghataure H. S., Davies R. D., Harrison B. A., Perley R., Crane P. C., Unger S. W., 1990, MNRAS, 246, 477

Polatidis A. G., Wilkinson P. N., Xu W., Readhead A. C. S., Pearson T. J., Taylor G. B., Vermeulen R. C., 1995, ApJS, 98, 1

Readhead A. C. S., Taylor G. B., Xu W., Pearson T. J., Wilkinson P. N., 1996, ApJ, 460, 612

Ruszkowski M., Begelman M. C., 2002, ApJ, 581, 223

Silver C. S., Taylor G. B., Vermeulen R. C., 1998, ApJ, 502, 229

Soker N., White R. E. III, David L. P., McNamara B. R., 2001, ApJ, 549, 832

Venturi T., Dallacasa D., Stefanachi F., 2004, A&A, 422, 515

White R. L., Becker R. H., 1992, ApJS, 79, 331

Wilkinson P. N., Polatidis A., Readhead A. C. S., Xu W., Pearson T. J., 1994, ApJ, 432, L87

Yee H. K. C., Ellingson E., Abraham R. G., Gravel P., Carlberg R. G., Smecker-Hane T. A., Schade D., Rigler M., 1996, ApJS, 102, 289

Zhao J.-H., Sumi D. M., Burns J. O., Duric N., 1993, ApJ, 416, 51

This paper has been typeset from a TEX/LATEX file prepared by the author.